International Journal of Pharmaceutics xxx (xxxx) 123855

Contents lists available at ScienceDirect

International Journal of Pharmaceutics

journal homepage: www.elsevier.com/locate/ijpharm

Preparation and characterization of new salts of tioconazole. Comparison of their dissolution performance

Aldana B. Moroni [a], Elena Pérez Mayoral [b], Diego F. Lionello [c], Daniel R. Vega [d], Teodoro S. Kaufman [a,*], Natalia L. Calvo [a,*]

[a] Área de Análisis de Medicamentos, Facultad de Ciencias Bioquímicas y Farmacéuticas, Universidad Nacional de Rosario e Instituto de Química Rosario (IQUIR. CONICET-UNR), Suipacha 531, S2002LRK, Rosario, Argentina

[b] Departamento de Química Inorgánica y Química Técnica, Universidad Nacional de Educación a Distancia, UNED, Urbanización Monte Rozas, Avenida Esparta s/n, Ctra. de Las Rozas al Escorial Km 5, 28232 Las Rozas-Madrid, Spain

[c] Departamento Física de la Materia Condensada, Gerencia de Investigación y Aplicaciones, Centro Atómico Constituyentes, Comisión Nacional de Energía Atómica e Instituto Jorge A. Sabato, Universidad Nacional General San Martín, Av. Gral. Paz 1499, B1650KNA San Martín, Buenos Aires, Argentina

[d] Departamento Física de la Materia Condensada, Gerencia de Investigación y Aplicaciones, Centro Atómico Constituyentes, Comisión Nacional de Energía Atómica y Escuela de Ciencia y Tecnología, Universidad Nacional General San Martín, Av. Gral. Paz 1499, B1650KNA San Martín, Buenos Aires, Argentina

ARTICLE INFO

Keywords:
Tioconazole
Salt formation
Solid-state characterization
Powder dissolution
Powder X-ray diffractometry
Thermal methods
Vibrational spectroscopy

ABSTRACT

Tioconazole is an effective antifungal agent with very low solubility in aqueous media, which limits its bioavailability and efficacy. Aiming to overcome the drug limitations by improving the solubility of this active pharmaceutical ingredient, solution precipitation techniques were employed to prepare four new crystalline salts, namely the mesylate, tosylate, maleate (1:1), and fumarate (1:1) hemihydrate. The thermal stabilities, dissolution properties, and structural characteristics of the solids were determined, and the study was extended to compare their properties with the already-known oxalate salt.

The structural characterization of the new phases was carried out using a multi-method approach, which included thermal (differential scanning calorimetry and thermogravimetry), diffractometric (powder X-ray diffraction), and spectroscopic (near-infrared and mid-infrared) methodologies. The determination of the melting point of the salts confirmed the findings made by thermal methods. Functional characteristics of the salts, involving their intrinsic dissolution rates were also determined.

It was found that the salts exhibited improved thermal stability and that the nature of the counterion modulated their dissolution characteristics. The salts displayed better intrinsic dissolution rates than the free base, to the point of being "highly soluble" according to the Biopharmaceutical Classification System. At pH 4.3, the sulfonic acid derivatives exhibited better dissolution rates than their carboxylic acid-derived counterparts, greatly improved regarding bare tioconazole. The results suggest that the salts have great potential to be used as replacements for the free base; in principle, careful salt selection may help to fulfill each solubility need for the different scenarios where the drug may be used.

1. Introduction

The efficacy of any given pharmacological treatment is strongly related to the solubility and dissolution rate of the active pharmaceutical ingredient (API) involved. Approximately 40 % of the drugs in the market and 70–90 % of the candidates in the drug pipeline are poorly soluble compounds; in addition, one-quarter of them exhibit low permeability.

Solubility is an important physicochemical property of pharmaceutical compounds (Di et al., 2012), that is considered at different stages of drug discovery and development (Alsenz and Kansy, 2007). Even modern blockbuster molecules face limitations in their application range because of their poor solubility and defective dissolution profiles. Furthermore, the use of high-throughput screening processes has resulted in the discovery and development of more lipophilic lead compounds (Jain et al., 2015). Therefore, one of the key challenges for successful pharmaceutical product development of poorly soluble drugs is

* Corresponding authors.
E-mail addresses: kaufman@iquir-conicet.gov.ar (T.S. Kaufman), calvo@iquir-conicet.gov.ar (N.L. Calvo).

https://doi.org/10.1016/j.ijpharm.2024.123855
Received 9 November 2023; Received in revised form 15 January 2024; Accepted 23 January 2024
0378-5173/

to achieve improvements in their solubility and dissolution profiles without modifying their molecular structure.

Azole antifungals are no exception. They are the most commonly used agents for the clinical treatment of both superficial and systemic fungal infections. However, many members of this family display poor water solubility, which limits their bioavailability and conditions their antifungal effects. Tioconazole (TCZ, Fig. 1) is one of the most widely used azole-type antifungal agents. This imidazole derivative is a white or almost white solid (Sanli et al., 2013), with a low melting point (80 °C) (Crisóstomo-Lucas et al., 2015). The aqueous solubility of the drug is very low (16.5 mg/L) (Moroni et al., 2023), being further reduced to 1.7 mg/L at pH 6.8 (phosphate buffer) (Drozd et al., 2021), and its log P (partition octanol: water) is 4.23–4.86 (Brown et al., 2021; Stratton et al., 2015); these characteristics limit its bioavailability and antifungal activity.

Solubility enhancement of the active pharmaceutical ingredient (API) is a practical solution that oftentimes results in faster dissolution rates, which in turn can yield a significant improvement on its in vivo performance. Currently, a wide array of strategies is available to enhance the solubility of poorly water-soluble compounds (Williams et al., 2013); among them, crystal engineering has acquired relevance as a convenient intervention approach to improve the mechanical, physicochemical, chemical, and functional properties of pharmaceutical solids.

Crystal engineering involves a wide array of technologies, ranging from particle size reduction leading to the formation of ultrafine particles to optimize the properties of an API, to the formation of salts, cocrystals (Weng et al., 2019), high-energy amorphous forms, and metastable polymorphs (Nowak et al., 2020). However, unlike the amorphous state, which must be stabilized by polymers or other additives (Moroni et al., 2023), salts and cocrystals offer two unique advantages, mainly related to their inherent stability and crystallinity.

Salt formation is the oldest method for improving the stability and solubility of ionizable API (Berge et al., 1977;Handbook of Pharmaceutical Salts, 2002), and also for tailoring their pharmacokinetics (Mithu et al., 2021). This classic approach is still one of the most popular alternatives, where aqueous solubility is favored by ionic and electrostatic interactions (Serajuddin, 2007). The use of charged counterions, also capable of establishing hydrogen bonding interactions with water, also favors solubility by improving the transport of the ionized drug to the aqueous medium.

TCZ is an ionizable molecule that possesses a crystalline structure; therefore, the formation of salts is an acceptable option, especially considering that the current solid-state landscape of the drug looks rather simple and remains largely unexplored. To date, there is no evidence that the drug exhibits polymorphism. On the other hand, the group of Perlovich used a liquid-assisted grinding approach to prepare the anhydrous (1:1) salts with oxalic, malonic, DL-tartaric, and fumaric acids, and a monohydrate salt (1:1:1) with DL-tartaric acid (Drozd et al., 2021). In addition, we have recently prepared the hydrochloride hemihydrate salt of tioconazole by solvent evaporation (Moroni et al., 2023).

In this study, we describe the preparation and physical characterization of four new salts of TCZ, namely mesylate (TCZ-Ms), tosylate (TCZ-Ts), maleate (TCZ-Mal, 1:1), and fumarate hemihydrate (TCZ-Fum•½H_2O, 1:1), as well as their intrinsic dissolution rate performance. A comparison of the functional profiles of the new salts with the previously prepared oxalate (TCZ-Ox, 1:1) salt is included and the results are discussed.

2. Materials and methods

2.1. API and chemicals

Pharmaceutical grade TCZ bulk drug was kindly donated by Panalab Laboratories (Buenos Aires, Argentina). Double distilled water was used. All solvents employed were of analytical grade.

2.2. Preparation of the TCZ salts

TCZ-Ox: Oxalic acid dihydrate (81.6 mg, 0.65 mmol) was added to a solution of TCZ (250.9 mg, 0.65 mmol) in MeOH, and the resulting solution was concentrated at 40 °C under reduced pressure, in a rotary evaporator. The so-formed translucid solid was re-dissolved in a MeOH: EtOAc solution (1:3, *v/v*, 18 mL) and concentrated again at 40 °C under reduced pressure. The solid was dried at room temperature. The thermal (DSC and TGA) and X-ray diffraction (PXRD) data of the salt were in agreement with the literature (Fig. S1A and S1C; Table S2) (Drozd et al., 2021).

TCZ-Fum•½H_2O: A solution of fumaric acid (66.8 mg, 0.58 mmol) in Et_2O (6 mL) was added to a stirred, refluxing solution of TCZ (222.9 mg, 0.58 mmol) in Et_2O (6 mL) containing water (10.5 μL, 0.58 mmol). The system was stirred at 200 rpm for 40 min, subsequently cooled with an ice bath for an additional 15 min, and then later left in the freezer overnight. The supernatant was carefully removed, and the solid residue was dried at room temperature.

TCZ-Mal: A solution of maleic acid (69.1 mg, 0.60 mmol) in Et_2O (4 mL) was added to a refluxing solution of TCZ (230.9 mg, 0.60 mmol) in Et_2O (6 mL). The resulting suspension was stirred at 200 rpm for 40 min, subsequently cooled with an ice bath for an additional 15 min, and then later left in the freezer overnight. The supernatant was carefully removed and the solid residue was dried at room temperature.

TCZ-Ms: Methanesulfonic acid ($MeSO_3H$, 0.067 mL, 1.04 mmol) was added to a solution of TCZ (400.3 mg, 1.04 mmol) in Et_2O (10 mL). The resulting solution was stirred overnight at room temperature when the solids were left to settle into a compact mass. The supernatant was removed and the solid residue was dried at room temperature.

TCZ-Ts: *p*-Toluenesulfonic acid monohydrate ($TsOH·H_2O$, 270 mg, 1.43 mmol) was added to a solution of TCZ (551 mg, 1.43 mmol) in MeOH (20 mL), and the resulting solution was concentrated at 40 °C under reduced pressure in a rotary evaporator. The so-formed solid was re-dissolved in a MeOH: EtOAc solution (1:2, *v/v*, 45 mL) and concen-

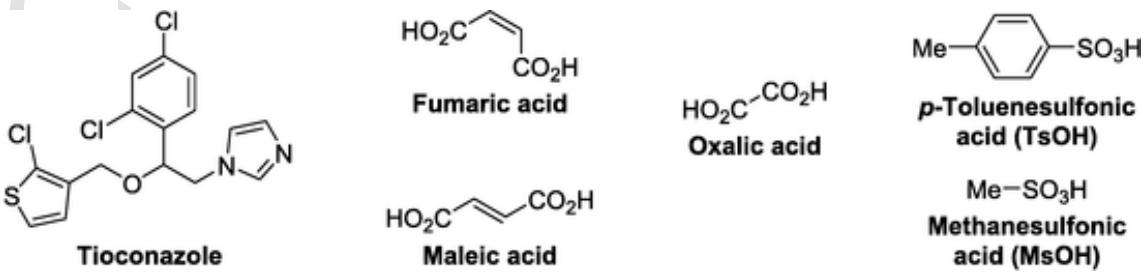

Fig. 1. Chemical structures of tioconazole base and the acid counterparts of this study, fumaric acid, maleic acid, oxalic acid, 4-toluenesulfonic acid, and methanesulfonic acid.

trated again at 40 °C under reduced pressure, yielding a white solid residue that was dried at room temperature.

2.3. Thermal methods

2.3.1. Differential scanning calorimetry

Differential scanning calorimetry (DSC) curves were obtained employing a Linseis PT1000 apparatus (Linseis Messgeraete GmbH, Selb, Germany) with the samples (~5 mg) placed in open aluminum pans and using an empty pan as a reference. The samples were heated 10 °C min^{-1} in the range 40–230 °C, under an inert atmosphere provided by a constant flow of nitrogen (130 mL^{-1}).

2.3.2. Thermogravimetric analysis

The thermogravimetric analysis (TGA) measurements were performed on a Shimadzu DTG-50 apparatus (Shimadzu Corp., Tokyo, Japan). The samples (~8 mg) were placed in alumina crucibles and heated at a rate of 10 °C min^{-1} from room temperature to 500 °C under nitrogen (flow rate = 20 mL min^{-1}), as the purge gas.

2.3.3. Hot stage microscopy

The thermal microscopy analyses were performed on a Leitz model 350 optical microscope (Ernst Leitz, GmbH, Wetzlar, Germany), fitted with a controllable heating plate and a 4 × Beion CMOS USB-digital camera (Shanghai Beion Medical Technology Co., Ltd., Shanghai, China) of 5.0 megapixels [resolution 2592 × 1944 (H × V)]. The solid samples were dispersed between two laboratory glasses and the system was placed into the heating plate cell, which was set under the objective lens of the microscope. The plate was heated at ~10 °C min^{-1} up to 10 °C below the temperature of interest; then, the heating rate was changed to ~1 °C min^{-1}. until passing the melting point. Solid state changes were detected visually and using the digital camera.

2.4. Vibrational spectroscopy studies

2.4.1. Mid-infrared spectroscopy

Mid-infrared (MIR) spectra were obtained with a GladiATR diamond-based ATR accessory, fitted with a Pike temperature control unit (Pike Technologies, Madison, USA), coupled to a Shimadzu Prestige 21 FTIR spectrometer (Shimadzu Corp., Kyoto, Japan). The spectra (20 scans at a resolution of 4 cm^{-1}) were acquired on ~20 mg samples along the 4000–600 cm^{-1} wavenumber range.

2.4.2. Near-infrared spectroscopy

The near-infrared (NIR) spectra were obtained with a NIRS DS2500 spectrometer (FOSS, Hillerød, Denmark) operating at room temperature in the reflectance mode, with the samples (~500 mg) placed in a circular quartz cell for solids. The spectral data were collected as an average of 7 scans per spectrum, at a resolution of 0.5 nm, in the spectral range 700–2500 nm.

2.5. Powder X-ray diffraction

The powder X-ray diffraction (PXRD) patterns were acquired at room temperature in a Panalytical Empyrean diffractometer (Malvern Panalytical Ltd., Malvern, UK) with a PixCel 3D detector operated at 40 kV and a current of 30 mA. The samples were placed in analuminum sample holder. The diffractograms were obtained over the 2θ range of 5–45°, at a step size of 0.026° and a counting time of 176 s, employing Cu Kα radiation (1.54184 Å) from a Ni-filtered source, a divergence incident slit of 0.5° and a soller slit of 0.04 rad.

2.6. Determination of the intrinsic dissolution rate

The test was performed employing the stationary disk method. The disks (surface area = 1.26 cm^2) were prepared by compression of the test powder (135 mg) in a suitable die (I.D. = 12.7 mm) with a Perkin Elmer (Perkin Elmer, Norwalk, USA) hydraulic press, applying 4 Ton $inch^{-2}$ for 20 min to ensure the obtention of disks that would not disintegrate during the test. A Hanson SR8-Plus dissolution station (Hanson Research, Chatsworth, USA), configured as USP apparatus II (paddles) was employed and the disks were inserted into a stainless steel holder so that only one face was exposed to the dissolution medium. The dissolution medium was double distilled water acidified to pH 4.3 (500 mL) at 37 ± 0.5 °C and the paddle rotation rate was 50 rpm (Rout et al., 2023).

Samples (3 mL) were taken at pre-specified times without replenishment; they were filtered, discarding the first drops, and suitable aliquots of the rest were properly diluted with dissolution medium. Calibration curves (n = 6; $r^2 > 0.996$) were concomitantly prepared by dilution of stock standard solutions of TCZ and the salts (~300 μg mL^{-1}) in acetonitrile. The assays for drug content were performed with a UV-1650PC UV–Vis spectrophotometer (Shimadzu Corp., Kyoto, Japan) fitted with a pair of quartz cells of 10 mm optical path length, employing absorbance measurements at 225 nm against a blank of dissolution medium. The intrinsic dissolution rate (IDR) was calculated from the slope of the straight line of the cumulative drug release graph, obtained by linear regression of the first six points (Serajuddin, 2007).

2.7. Data analysis and graphics software

Chemical structures were drawn with ChemOffice v.21 (PerkinElmer Informatics, Waltham, USA). Graphs and statistical data analysis were performed using Origin v.8.5 (OriginLab Co., Northampton, USA).

3. Results and discussion

3.1. Preparation of the solid-state forms

According to its chemical structure (Fig. 1), TCZ has three H-bond acceptors (two nitrogen atoms of the imidazole ring and an ether oxygen atom) but lacks polar H-bond donor groups able to form synthons with acid groups, which are common in multicomponent crystal systems. These features and the fact that the drug is a weak base (pK_a: 6.51–6.61)[4] support both, the possibility of obtaining salts and salt hydrates, where hydration may serve to fulfill the stabilization requirements of the supramolecular crystal system.

The "rule of 3" is a well-accepted paradigm that deals with the proton transfer ability of certain species. This indicates that a salt should be expected in ionizable species when the difference between the pK_a of the API and the counterions involved (ΔpK_a) is greater than 3 units [$\Delta pK_a = pK_{a\,(base)} - pK_{a\,(acid)} > 3$] (Childs et al., 2007). More recently, systematic studies have estimated that at $\Delta pK_a = 3$, the likelihood of salt formation is approximately 80 %. Accordingly, salt formation can also take place when $\Delta pK_a < 3$, although with a much lower probability; however, when $\Delta pK_a \sim 1$ cocrystal formation is favored (Cruz-Cabeza, 2012).

Therefore, during the salt formation process of TCZ, an acid-base reaction takes place with the acid component, where a proton is hypothetically transferred from the most acidic group of the latter to the most basic nitrogen site in TCZ.

According to the available data (Table S1), methanesulfonic acid and *p*-toluenesulfonic acid are strong enough sulfonic acids to grant salt formation, whereas salts could also be expected to form from the dicar-

boxylic acids maleic, fumaric, and oxalic, which still have pK_a 1 values low enough to ensure that the "rule of 3" is fulfilled in all cases.

The salts were successfully prepared and obtained as white solids by adding one molar equivalent of the acids, as solids or in solution, to solutions of TCZ in MeOH or Et_2O and recovering the precipitated salts or concentrating the solutions until suitable solids were formed. In our hands, the formation of the previously reported anhydrous fumarate salt (TCZ-Fum) as a pure phase in ^{i}PrOH and under different conditions (concentration, time, and temperature) was not possible; however, in the presence of a molar equivalent of water, a mixture of TCZ and fumaric acid in Et_2O conveniently and consistently afforded the hemihydrate (TCZ-Fum•½H_2O) as a pure new phase.

3.2. Physical characterization of the tioconazole salts

3.2.1. Thermal analysis (DSC and TGA) and melting point

This study (Figs. 2 and S2, and Table S2) was carried out to characterize the thermal stability of the compounds, to understand the different events that take place upon heating and to detect the presence of water. The salts exhibited quite different thermal properties and, in general, displayed higher thermal stability than their precursor TCZ, the DSC curve of which was included for comparison (Fig. 2A.c–D.c). The thermal behavior of TCZ-Ox (Fig. S1A, Table S2), prepared for performance comparison, agreed with the literature (Drozd et al., 2021).

In the studied temperature range, TCZ displayed a single melting event with T_{onset}: 79.1 °C (T_{peak}: 83.5 °C) (Calvo et al., 2019), whereas the dicarboxylic acid derivatives TCZ-Mal and TCZ-Fum•½H_2O (Fig. 2A and B) exhibited two endotherms each, associated to their melting and decomposition events, respectively (Rout et al., 2023). These endotherms were separated by a small exothermic event, probably related to the crystallization of the unstable melt, which became involved in decomposition upon further heating. These observations were supported by the corresponding TGA curves, which revealed that the decomposition of the dicarboxylic acid-derived salts took place as a two-stage process (besides the water loss event), where the first step seemed to be related to the decomposition of the anion moiety.

In agreement with the general observations, the DSC curve of TCZ-Mal (Fig. 2A.a) displayed an endothermic event corresponding to the melting of the solid with T_{onset}: 110.8 °C; Δh: −82 J g^{-1} (T_{peak}: 114.6 °C), and a decomposition endotherm, which began at 144 °C. The simplicity of the DSC curve of the salt contrasted with that of maleic acid (Fig. 2A.b), which displayed a complex endotherm in the region 137–193 °C, that included prominent signals at 144.9, 159.4, and 160.9 °C.

On the other hand, the characteristic melting endotherm of the TCZ-Fum•½H_2O was observed as a rather broad single signal in the DSC curve with a T_{onset}: 74.3 °C, a maximum at 85.4 °C and a small shoulder (Fig. 2B.a). This event was accompanied by concomitant dehydration, as evidenced by the thermogravimetric curve (Fig. 2B.d), where it displayed a mass loss of 1.76 % (required for 0.5 H_2O: 1.76 %).

Interestingly, the peak reported by the group of Perlovich for the anhydrous TCZ-Fum (T_{onset}: 117.3 °C and T_{peak}: 123.3 °C) was not observed in the DSC curve of the hemihydrate, suggesting that no transition from the hemihydrate to the anhydrous phase reported by Perlovich takes place under the studied conditions.

Several models have been proposed for the dehydration mechanisms. TCZ-Fum•½H_2O undergoes destructive release of water without reorganization of the dehydrated product, which probably results in an amorphous material. This behavior responds to Class I of Petit and Coquerel's classification scheme Petit and Coquerel (1996). Considering that the water evolution is concomitant with a comprehensive and complete melting event, the hemihydrate salt could also be graded as Type 6 in the more complex Galwey's approach, which also takes into account kinetic and rate-controlling phenomena (Jørgensen et al., 2009).

On the other hand, the sulfonic acid salts TCZ-Ms and TCZ-Ts (Fig. 2C.a and 2D.a) were thermally more stable and their DSC curves were simpler, exhibiting a single endotherm each. TCZ-Ms displayed a melting event with T_{onset}: 201.6 °C; Δh: −116 J g^{-1} (T_{peak}: 205.7 °C) and its TGA curve indicated that the salt is thermally stable up to 290 °C, well beyond its melting point.

The DSC curve of TCZ-Ts (Fig. 2D.a) displayed a melting endotherm with T_{onset}: 134.3 °C; Δh: −56 J g^{-1} (T_{peak}: 139.4 °C). This salt is anhydrous, as indicated by the corresponding thermogravimetric curve (Fig. 2D.d) which also revealed that it is thermally stable up to 280 °C.

According to the thermogravimetric data, except for TCZ-Fum•½H_2O (which included an initial dehydration process), all the

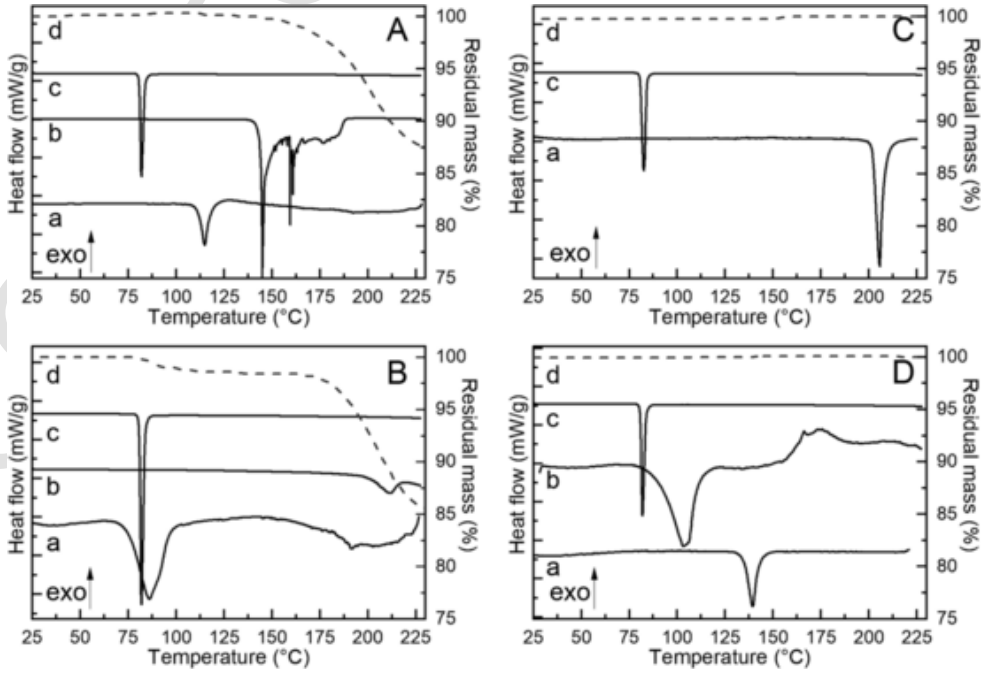

Fig. 2. Thermal analysis of the TCZ salts and their precursors in the range 25–230 °C. (A) TCZ-Mal; (B) TCZ-Fum•½H2O; (C) TCZ-Ms; (D) TCZ-Ts. DSC curves: a) Salt; b) Acid component (MsOH is a liquid); c) TCZ. d) Thermogravimetric curve (dashed line) of the salt.

first thermal events observed in the DSC curves were not accompanied by significant weight loss in the corresponding TGA curves.

Melting requires the rupture of the crystal structure, whereas degradation also includes bond breaking. The thermal decomposition temperature at 5 % mass loss (T_{d5}) is considered a suitable indicator and a representative parameter to evaluate differences in compound stability (Worzakowska et al., 2023). Accordingly, employing the data displayed in Fig. S2 a thermal stability order was established, where TCZ-Ms (T_{d5}: 327 °C) proved to be the most stable, followed by TCZ-Ts (T_{d5}: 310 °C), and then by the organic dicarboxylic acid-derived salts, TCZ-Fum•½H_2O, TCZ-Mal, and TCZ-Ox. The latter group exhibited T_{d5} in a rather narrow range of 193–202 °C; however, among them, TCZ-Ox displayed the highest melting point (160 °C), at a temperature that also marked the beginning of its decomposition.

The events attributed to the melting episodes of the pure crystalline phases were in agreement (Table S2) with the observations made in the corresponding thermomicroscopy experiments (Fig. 3). These also revealed that the carboxylic acid salts displayed birefringence under illumination with polarized light (Fig. 3A-C.b), which disappeared upon melting (Fig. 3A-C.d), whereas no birefringence could be observed in both sulfonic acid salts, which were considered as optically isotropic.

3.2.2. Spectroscopic analysis (NIR and MIR)

3.2.2.1. NIR spectra. The salts displayed unique spectra, generally characterized by some new bands, along with shifted peaks of different intensities with regard to their precursors (Figs. 4 and S1D). The positions and assignments of the most relevant absorption bands are summarized in Table S3. TCZ exhibited two distinguishable signals at 1112 and 1210 nm, corresponding to the second harmonics of the C–H aromatic (ArCH) and secondary or tertiary carbons, respectively, whereas the dicarboxylic acids displayed their second harmonics of the alkene C–H (–HC = CH) band at 1131 nm (fumaric) and 1137 nm (maleic). However, the carboxylic acid salts exhibited a couple of characteristic bands in that region, one of them in a narrow range (1129–1132 nm), whereas the other at 1088 nm for TCZ-Mal (Fig. 4A.c), 1092 nm for TCZ-Fum•½H_2O (Fig. 4B.c), 1096 nm for TCZ-Ox (Fig. S1D.c) and at 1100 nm for the sulfonic acid salts.

Analogously, the signals of TCZ peaking at 1394 and 1456 nm (methylene C–H) appeared slightly blue-shifted in the carboxylic acid salts to 1373 and 1402 nm in TCZ-Mal, 1376 and 1438 in TCZ-Fum•½H_2O, and 1380 and 1408 nm in TCZ-Ox, respectively. However, the shift was less pronounced for the sulfonic acid derivatives [TCZ-Ms: 1379 and 1445 nm (Fig. 4C.c); TCZ-Ts: 1384 and 1441 nm (Fig. 4D.c)].

The distinguished peak of TCZ centered at 1634 nm corresponds to the first overtone of the ArC–H stretching vibration (Rout et al., 2023); it is also present in the spectrum of TsOH (1672 nm), which carries an aromatic ring, but not in those of the remaining acids used in this study. The salts, however, display broad absorption bands in this region (1602–1665 nm), as multiple and often overlapped peaks with lower intensity. Probably, these bands reflect conformational changes resulting from the protonation of the distal imidazole nitrogen atom in TCZ as a result of salt formation.

The spectrum of TCZ also has a broader companion band in the 1715–1815 nm region, which can be assigned to the first overtone of the C–H vibration of the CH_2 groups. The salts also exhibit absorption in this zone; however, the carboxylic acid-derived salts display a more simple pattern, characterized by a single main peak in the region 1708–1711 nm (1721 nm for TCZ-Ox), unlike the sulfonic acid derivatives, which have several small peaks in this zone, spanning up to 1798 nm. Low-intensity signals observed at 1224, 1462, and 1810 nm were hints suggesting that the fumarate salt is a hydrate, confirming the results obtained by TGA.

Finally, it is worth noting that the spectra of all compounds contained a characteristic and complex pattern of absorptions in the 2150–2500 nm region, corresponding to HC–C and HC = C combination bands; however, their intensities were stronger than those of the simple

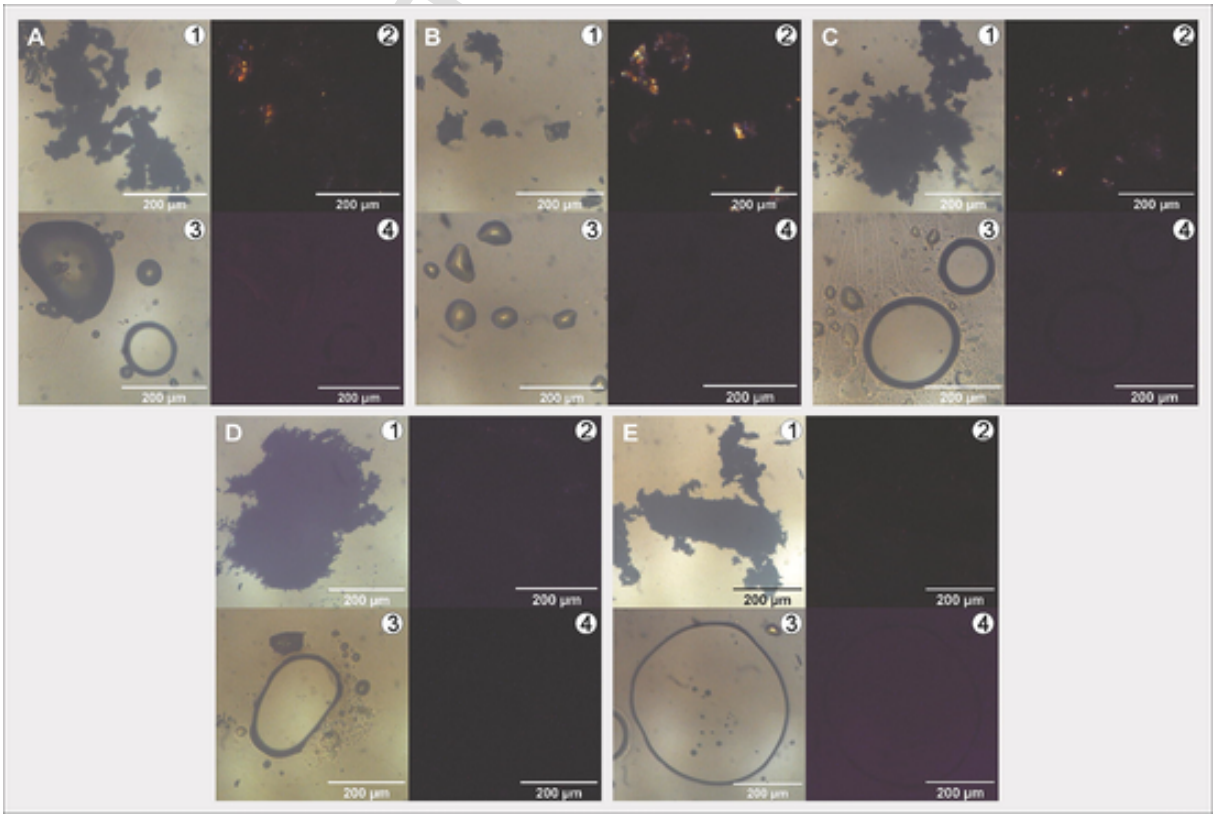

Fig. 3. Thermomicroscopic analysis of the TCZ salts. (A) TCZ-Mal; (B) TCZ-Fum•½H_2O; (C) TCZ-Ox; (D) TCZ-Ms and (E) TCZ-Ts. (1) and (2) Before the melting point; (3) and (4) After the melting point; (1) and (3) with white light; (2) and (4) under polarized light.

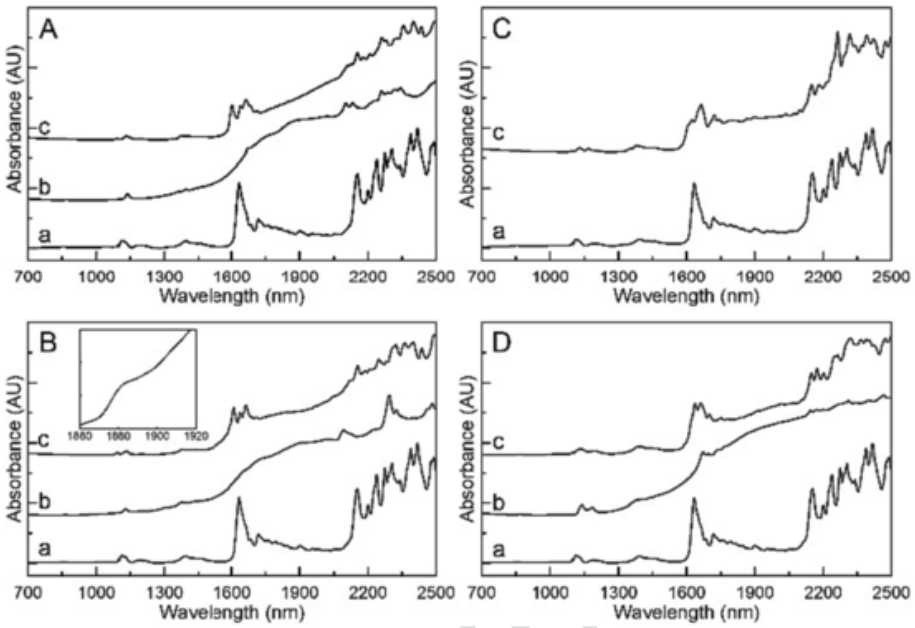

Fig. 4. Near-infrared absorption spectra of the precursors TCZ (a) and acids (b), and their corresponding salts (c). (A) TCZ-Mal; (B) TCZ-Fum•½H_2O (inset: expansion plot of the 1880–1920 nm region); (C) TCZ-Ms; (D) TCZ-Ts. Methanesulfonic acid is a corrosive liquid and its spectrum was not included.

signals found in the acid precursors and weaker than those found in TCZ.

3.2.2.2. MIR spectra. Infrared spectroscopy is a simple and convenient analytical tool for detecting chemical interactions, including those leading to the formation of new chemical entities, being a valuable technique for their identification. Band shifting, broadening, and the appearance of new absorptions, or changes in band intensity resulting from modifications of their vibrational energies (Aitipamula et al., 2014), are useful indicators of the presence of such interactions. Therefore, this spectroscopy is suitable for assessing proton transfer and confirming salt formation, being often used to differentiate between salt and co-crystal formation based on the ionization state of acidic and basic components (da Silva et al., 2016).

For diagnostic purposes, it has been shown that carboxylic salt formation is evident through the appearance of signals assignable to carboxylate anions which have a strong band below 1600 cm^{-1} and a weaker symmetrical band near 1400 cm^{-1}, corresponding to the asymmetrical and symmetrical stretching bands of the carboxylate unit (Hiendrawan et al., 2017). In contrast, the formation of co-crystal species is revealed by a blue shift of the carbonyl moiety of the carboxylic acid, to absorb in the range of 1700–1730 cm^{-1}.

The salts were obtained by precipitation from saturated solutions prepared with equimolar amounts of their precursors. Because some dicarboxylic acids were employed as precursors, potentially enabling the generation of 1:1 and 2:1 (acid:TCZ) salts, and considering the possibility of hydrate formation, they were characterized, along with their precursors, by MIR spectroscopy (Figs. 5 and S4). The positions and assignments of the most relevant absorption bands are summarized in Table S4. The spectra of the precursors were in good agreement with the literature; they are described for the sake of comparison with the corresponding salts, which displayed unique spectra that enabled their identification. TCZ also exhibited a complex infrared spectrum, characterized by bands related to its main functional groups (Serajuddin, 2007).

TCZ-Mal.- The spectrum of the new solid exhibited a new band at 1690 cm^{-1}, which was attributed to the $\nu_{C=O}$ of the free CO_2H moiety of maleic acid in the salt (Fig. 5A.c), and additional signals at 1576 and 1435 cm^{-1}, which were assigned to the antisymmetric and symmetric stretching modes of the CO_2^- group, confirming its presence in the salt. These signals have been employed as evidence of carboxylic acid deprotonation (Florio and Zwier, 2003).

In addition, peaks corresponding to the symmetric and asymmetric ν_{NH} vibrations of the protonated imidazole were visible at 3105 and 3048 cm^{-1}. In addition, the O–H stretching of the carboxylic acid spanned the 3200–2170 cm^{-1} region, also confirming the formation of the salt, whereas no sign of the ν_{O-H} band related to water was observed, confirming that the salt is anhydrous. Concomitantly, the band of TCZ at 1503 cm^{-1} ($\nu_{C=N}$ imidazole), was missing in the salt, possibly being displaced to lower wavenumbers, and the C-S found in TCZ at 692 cm^{-1} (Fig. 5A.a) was observed at 702 cm^{-1} in the salt.

TCZ-Fum•½H_2O.- The salt (Fig. 5B.c) displayed the ν_{OH} band of the carboxylic acid in the range 3250–2150 cm^{-1}. This detail has been used as an indicator of salt formation (Mondal et al., 2017), being useful to confirm that even though fumaric acid is the weakest acid in this study (pK_a1: 3.02; ΔpK_a1: 3.53), the new phase is not a co-crystal. These signals were overlapped with the ν_{OH} of water (~3200 cm^{-1}). In addition, it showed a peak at 1712 cm^{-1}, corresponding to $\nu_{C=O}$ of the free carboxylic acid moiety, and a couple of bands at 1577 and 1466 cm^{-1}, with smaller intensity when compared to the dicarboxylic acid, which was assigned to the antisymmetric and symmetric stretching vibrations of the CO_2^- group ($\nu_{C=O}$), respectively (Diniz et al., 2012; Aitipamula et al., 2014). The decrease in the intensity and shifting in the values are indicative that the C=O moiety is participating in a strong hydrogen bond formation.

TCZ-Ox.- This salt has been previously prepared by the group of Perlovich (Drozd et al., 2021); however, since its MIR spectrum remains unknown, it is presented and discussed here for the first time (Fig. S1B). The salt displayed a broad signal at 1710 cm^{-1}, assignable to $\upsilon_{C=O}$ of the free carboxylic acid and a wide band in the 3200–2000 cm^{-1} region (υ_{OH}). No signs of hydration water were detected, confirming the anhydrous nature of the salt. Despite small changes in position and intensity, the bands in the 1600–1200 cm^{-1} zone were reminiscent of those found in the same region in the spectrum of TCZ, whereas sharp intense peaks at 823 and 752 cm^{-1} also resembled those observed at slightly lower wavenumbers in TCZ (814 and 735 cm^{-1}).

TCZ-Ms.- The salt (Fig. 5C.c) was characterized by the appearance of new bands at 1233 and 1032 cm^{-1}, associated with vibrations of the

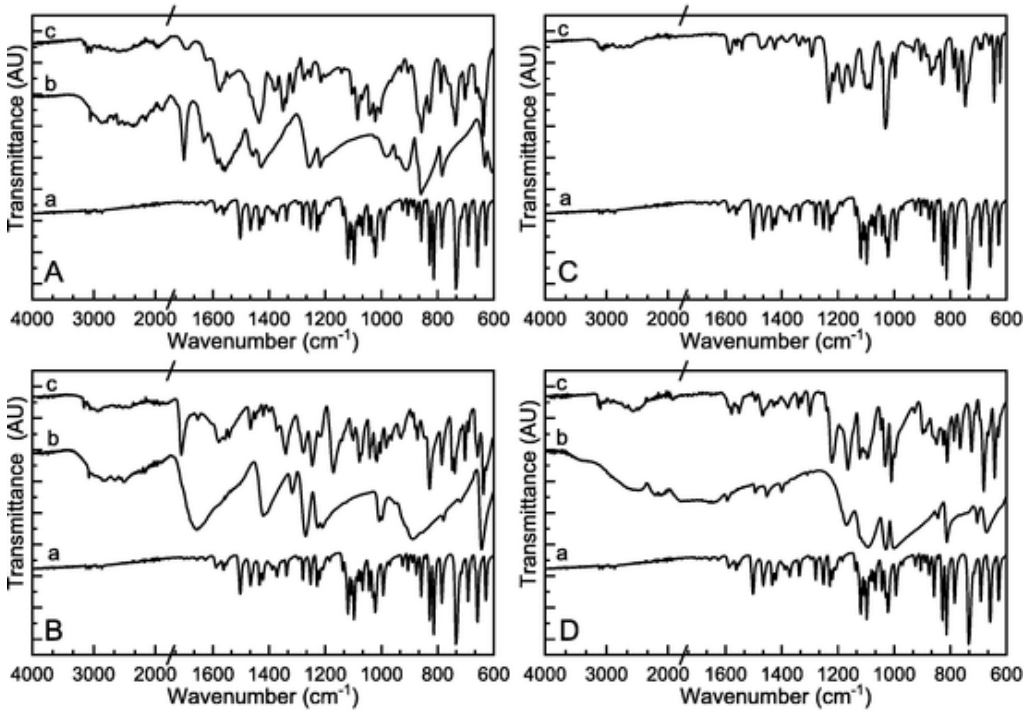

Fig. 5. Mid-infrared absorption spectra of TCZ (a) and acids (b), and their corresponding salts (c). (A) TCZ-Mal; (B) TCZ-Fum•½H_2O; (C) TCZ-Ms; (D) TCZ-Ts. Methanesulfonic acid is a corrosive liquid and its spectrum was not included.

antisymmetric and symmetric S-O stretching modes of the mesylate anion. In addition, a signal assignable to the N–H stretching vibration of the protonated imidazole moiety was detected at 3178 cm^{-1}, with concomitant disappearance of the band at 1505 cm^{-1}, characteristic of the $\nu_{C=N}$ of the imidazole ring. The salt is anhydrous, as it stems from the lack of a specific ν_{O-H} band. In addition, the zone of the $\nu_{C=C}$ vibrations corresponding to the substituted aromatic rings (1600–1300 cm^{-1}), is reminiscent of that of the free base (Fig. 5C.a), except that some bands are slightly red-shifted.

TCZ-Ts.- In analogy with the mesylate, TCZ-Ts (Fig. 5D.c) displayed two characteristic new bands at 1221 and 1011 cm^{-1}, which correspond to the antisymmetric and symmetric stretching vibrations of the S-O bond of the tosylate anion. In addition, a signal assignable to the N–H stretching vibration of the protonated imidazole moiety was detected at 3132 cm^{-1}, with concomitant disappearance of the band at 1505 cm^{-1}, characteristic of $\nu_{C=N}$ of the imidazole ring. The lack of an ν_{O-H} band confirmed that the salt is anhydrous. Finally, the region 1600–1300 cm^{-1} which contains the $\nu_{C=C}$ vibrations of the substituted aromatic rings, bore great similarity with that of the mesylate.

3.2.3. Powder X-ray diffractometry

The uniqueness of the crystalline phases and their purity were evaluated by PXRD, confirming that the experimental diffractograms of the starting materials were consistent with those reported in the literature (Fig. 6) (Bolla and Nangia, 2018; Espinoza-Lara et al., 2013). In addition, it was observed that the solids are crystalline, yielding diffractograms with sharp and well-defined diffractions, where each salt exhibited a unique array of characteristic peaks (Table S5), free of signals of its precursor, indicating in each case the formation of a new solid form.

The diffractograms of the new salts and that of the oxalate (Fig. S1C) are clearly different; therefore, they can be unambiguously distinguished, and differentiated as novel individual entities.

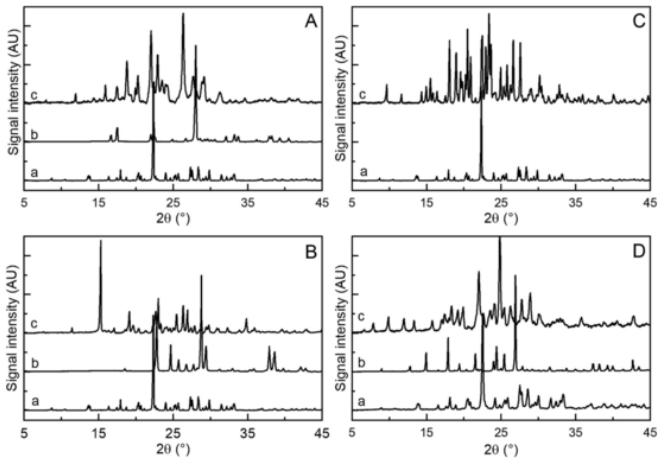

Fig. 6. Powder X-ray diffractograms of the precursors, TCZ (a) and acids (b), and their corresponding salts (c). (A) TCZ-Mal; (B) TCZ-Fum•½H_2O; (C) TCZ-Ms; (D) TCZ-Ts. Methanesulfonic acid is a liquid.

3.3. Stability of the salts

The stability of the new phases was studied under ambient conditions (25 °C and 75 % RH) for at least 6 months. According to MIR and DSC analyses, both sulfonic acid derivatives, as well as the maleate salt, did not display any observable change. However, periodic analyses of TCZ-Fum•½H_2O evidenced that the salt undergoes a slow dehydration (Fig. S3), resulting in a new phase (T_{onset}: 113.6 °C; T_{peak}: 118.7 °C), reminiscent of that previously described by the group of Perlovich (T_{onset}: 117.3 °C; T_{peak}: 123.3 °C) (Drozd et al., 2021).

3.4. Functional characterization. Intrinsic dissolution rate

The intrinsic dissolution rate (IDR) is defined as the amount of drug dissolved per unit time per unit area. It can be used not only for select-

ing optimal polymorphs and salts of an API but also to improve the prediction of drug behavior under dynamic conditions, such as those found in the gastrointestinal tract (Issa and Ferraz, 2011). The IDR determination is also a simple and convenient alternative to determine the Biopharmaceutical Classification System (BCS) solubility class (high/low) of a drug under different pH conditions when a 0.1 mg cm^{-2} min^{-1} cut-off is employed (Yu et al., 2004).

In order to evaluate the performance of the salts, IDR studies were carried out under our previously reported conditions (Serajuddin, 2007; Rout et al., 2023), using TCZ as a comparator drug (IDR: 5.3 × 10^{-3} mg cm^{-2} min^{-1}). As shown in Fig. 7, the carboxylic acid derivatives displayed the lowest dissolution rate [TCZ-Fum•½H_2O: (2.49 ± 0.20) × 10^{-1} mg cm^{-2} min^{-1}; TCZ-Mal: (4.31 ± 0.04) × 10^{-1} mg cm^{-2} min^{-1}], whereas among the sulfonic acid derivatives TCZ-Ms (18.95 ± 0.48) × 10^{-1} mg cm^{-2} min^{-1}) proved to initiate dissolution considerably faster than its congener TCZ-Ts (6.27 ± 0.21) × 10^{-1} mg cm^{-2} min^{-1}). Comparatively, TCZ-Ox exhibited a low value [IDR: 2.42 ± 0.24) × 10^{-1} mg cm^{-2} min^{-1}], being statistically equivalent to TCZ-Fum•½H_2O, the less soluble of the new phases (Table S6).

In the current case, the counterions of the new salts unequivocally modulated their IDR behavior, which spanned over one order of magnitude. The IDR values of the salts were approximately 45–355 times that of TCZ free base; however, the IDR value of TCZ-Ms was still ~6.2 times lower than that recorded for TCZ-HCl•½H_2O (Serajuddin, 2007).

The group of Perlovich performed powder dissolution studies with TCZ and five of its salts and cocrystals in phosphate buffer at pH 6.8 (Drozd et al., 2021). Interestingly, their observed concentrations of dissolved TCZ were low (<0.75 mg mL^{-1}), peaked at 30–40 min, exhibited a parachute effect, and finally fell below 0.1 mg mL^{-1} after 6 h. Among the tested compounds, TCZ-Ox displayed the best dissolution performance.

Under our test conditions, the parachute effect was not observed, presumably as a result of better solubility of the compounds, which exhibited a performance at least similar to that of TCZ-Ox. Furthermore, considering an IDR cut-off value of 0.1 mg cm^{-2} min^{-1} for classifying the solubility of drugs, as suggested by Kaplan (Kaplan, 1972), these results clearly indicate that salt formation with dicarboxylic and sulfonic acids notably improves the IDR of the TCZ derivatives to the point of converting them into BCS "high solubility" drugs.

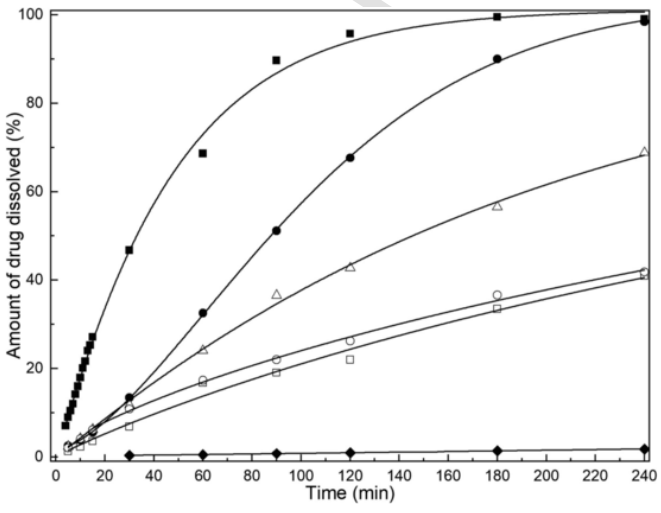

Fig. 7. Intrinsic drug dissolution rates of TCZ-Ms (■), TCZ-Ts (●), TCZ-Mal (Δ), TCZ-Fum•½H_2O (○), TCZ-Ox (□), and TCZ (♦).

4. Conclusions

Structural and performance diversity were obtained through the preparation of four new salts of TCZ, namely maleate, fumarate hemihydrate, tosylate, and mesylate along with the known acid oxalate salt. The compounds were physically characterized by a multi-technique approach involving thermal (DSC, TGA, melting point), vibrational spectroscopic (near- and mid-infrared), and diffractometric (X-ray powder diffractometry) means. In addition, the intrinsic dissolution rates of all of the salts were determined, as a functional characterization.

Employing the 5 % mass loss in the thermogravimetric curves as a thermal stability indicator, and disregarding the water loss of TCZ-Fum•½H_2O, the sulfonic acid salts excelled, displaying better thermal stability than TCZ free-base. TCZ-Ms proved to be the most stable, followed by TCZ-Ts, TCZ-Fum•½H_2O, TCZ-Mal, and TCZ-Ox in this order. In addition, except TCZ-Fum•½H_2O which underwent slow dehydration, the salts were stable for at least 6 months at ambient temperature and 75 % RH.

All the dicarboxylic acid-derived compounds began decomposition shortly after melting, and except for TCZ-Fum•½H_2O, the melting point of the salts was higher than that for TCZ. In addition, the acid fumarate hemihydrate salt displayed a dehydration event that overlapped with its melting process.

It was also observed that the new compounds displayed unique spectroscopic and diffractometric patterns, different from those of their precursors, which may conveniently enable their easy identification. The diffractometric data of TCZ-Ox were in agreement with the literature, whereas its MIR and NIR spectra were reported for the first time.

From the functional viewpoint, the IDR of the salts spanned over a range of 45–355 times that of TCZ and followed a trend reminiscent of those of their thermal stabilities (T_{d5}) and pK_a values of the acid precursors. The dicarboxylic acid derivatives displayed lower IDR values than their sulfonic acid counterparts and TCZ-Ms proved to initiate dissolution considerably faster than the tosylate. Thus, the nature of the anions proved to modulate the IDR of the salts, all of which can be regarded as BCS "highly soluble", in contrast with TCZ. According to these results, the more stable maleate, tosylate and mesylate salts may find use as replacements for TCZ when a more soluble drug is required, suggesting that their potential to be employed for marketing purposes is of capital importance.

CRediT authorship contribution statement

Aldana B. Moroni: . **Elena Pérez Mayoral:** Writing – review & editing, Supervision, Resources. **Diego F. Lionello:** . **Daniel R. Vega:** . **Teodoro S. Kaufman:** . **Natalia L. Calvo:** Writing – review & editing, Writing – original draft, Visualization, Validation, Supervision, Resources, Methodology, Investigation, Formal analysis, Conceptualization.

Declaration of competing interest

The authors declare that they have no known competing financial interests or personal relationships that could have appeared to influence the work reported in this paper.

Data availability

Data will be made available on request.

Acknowledgments

The authors gratefully acknowledge Consejo Nacional de Investigaciones Científicas y Técnicas (CONICET, PIP 2021-0765), Agencia Nacional de Promoción Científica y Tecnológica (ANPCyT, PICT 2019-

1155), Agencia Santafesina de Ciencia, Tecnología e Innovación (ASaCTeI, Project IO2019-302, BMG-N-2021-134) for financial support. ABM is also thankful to CONICET for her Doctoral fellowship, and Fundación Carolina is acknowledged for supporting a short stay of NLC at the UNED (Madrid, Spain). BSc. Cynthia Hucailuk and Cristian Oubiña are acknowledged for technical assistance with PXRD, and TGA determinations.

Appendix A. Supplementary material

Supplementary data to this article can be found online at https://doi.org/10.1016/j.ijpharm.2024.123855.

References

Aitipamula, S., Wong, A.B.H., Chow, P.S., Tan, R.B.H., 2014. Pharmaceutical salts of haloperidol with some carboxylic acids and artificial sweeteners: hydrate formation, polymorphism and physicochemical properties. Cryst. Growth Des. 14, 2542–2556. https://doi.org/10.1021/cg500245e.

Aitipamula, S., Chow, P.S., Tan, R.B.H., 2014. Crystal engineering of tegafur cocrystals: structural analysis and physicochemical properties. Cryst. Growth Des. 14, 6557–6569. https://doi.org/10.1021/cg501469r.

Alsenz, J., Kansy, M., 2007. High throughput solubility measurement in drug discovery and development. Adv. Drug Deliv. Rev. 59, 546–567. https://doi.org/10.1016/j.addr.2007.05.007.

Berge, S.M., Bighley, L.D., Monkhouse, D.C., 1977. Pharmaceutical salts. J. Pharm. Sci. 66, 1–19. https://doi.org/10.1002/jps.2600660104.

Bolla, G., Nangia, A., 2018. Novel pharmaceutical salts of albendazole. CrystEngComm 20, 6394–6405. https://doi.org/10.1039/C8CE01311J.

Brown, E.D., El Zahed, S.S., Farha, M.A., French, S., Kumar, G., 2021. Physicochemical and structural parameters contributing to the antibacterial activity and efflux susceptibility of small-molecule inhibitors of Escherichia coli. Antimicrob. Agents Chemother. 65, E01925–E02020. https://doi.org/10.1128/AAC.01925-20.

Calvo, N.L., Alvarez, V.A., Lamas, M.C., Leonardi, D., 2019. New approaches to identification and characterization of tioconazole in raw material and in pharmaceutical dosage form. J. Pharm. Anal. 9, 40–48. https://doi.org/10.1016/j.jpha.2018.11.006.

Childs, S.L., Stahly, G.P., Park, A., 2007. The salt-cocrystal continuum: the influence of crystal structure on ionization state. Mol. Pharm. 4 (2007), 323–338. https://doi.org/10.1021/mp0601345.

Crisóstomo-Lucas, C., García-Holley, P., Hernández-Ortega, S., Sánchez-Bartéz, F., Gracía-Mora, I., Barba-Behrens, N., 2015. Structural characterization and cytotoxic activity of tioconazole coordination compounds with cobalt(II), copper(II), zinc(II) and cadmium(II). Inorg. Chim. Acta 438, 245–254. https://doi.org/10.1016/j.ica.2012.11.026.

Cruz-Cabeza, A.J., 2012. Acid-base crystalline complexes, the pKa rule. CrystEng-Comm. 14, 6362–6365. https://doi.org/10.1039/C2CE26055G.

da Silva, C.C., Guimaraes, F.F., Rubeiro, L., Martins, F.T., 2016. Salt of cocrystal of salt? Probing the nature of multicomponent crystal forms with infrared spectroscopy. Spectrochim. Acta A 167, 89–95. https://doi.org/10.1016/j.saa.2016.05.042.

Di, L., Fish, P.V., Mano, T., 2012. Bridging solubility between drug discovery and development. Drug Discov. Today 17, 486–495. https://doi.org/10.1016/j.drudis.2011.11.007.

Diniz, L.F., Franco, C.H.J., Silva, D.F., Martins, L.S., Carvalho, Jr, P.S., Souza, M.A.C., Reis, N.F.A., Fernandes, C., Diniz, R., 2012. Multicomponent ionic crystals of diltiazem with dicarboxylic acids toward understanding the structural aspects driving the drug-release. Int. J. Pharm. 605, 120790. https://doi.org/10.1016/j.ijpharm.2021.120790.

Drozd, K.V., Manin, A.N., Boycov, D.E., Churakov, A.V., Perlovich, G.L., 2021. Pharmaceutical multicomponent crystals of antifungal drugs with improved dissolution performance. Cryst. Growth Des. 21, 7285–7297. https://doi.org/10.1021/acs.cgd.1c01139.

Espinoza-Lara, J.C., Guzmán-Villanueva, D., Arenas-García, J.I., Herrera-Ruiz, D., Rivera-Islas, J., Román-Bravo, P., Morales-Rojas, H., Höpfl, H., 2013. Cryst Growth Des. 13, 169–185. https://doi.org/10.1021/cg301314w.

Florio, G.M., Zwier, T.S., 2003. Theoretical modeling of the OH stretch infrared spectrum of carboxylic acid dimers based on first-principles anharmonic couplings. J. Chem. Phys. 118, 1735–1746. https://doi.org/10.1063/1.1530573.

Handbook of Pharmaceutical Salts: Properties, Selection, and Use. Eds.: Stahl, P.H., Wermuth, C.G., Verlag Helvetica Chimica Acta, Zürich, Switzerland, 2002. ISBN 3-906390-26-8.

Hiendrawan, S., Widjojokusumo, E., Veriansyah, B., Tjandrawinata, R.R., 2017. Pharmaceutical salts of carvedilol: polymorphism and physicochemical properties. AAPS PharmSciTech 18, 1417–1425. https://doi.org/10.1208/s12249-016-0616-x.

Issa, M.G., Ferraz, H.G., 2011. Intrinsic dissolution as a tool for evaluating drug solubility in accordance with the biopharmaceutics classification system. Dissolut. Technol. 18, 6–13. https://doi.org/10.14227/DT180311P6.

Jain, S., Patel, N., Lin, S., 2015. Solubility and dissolution enhancement strategies: current understanding and recent trends. Drug Dev. Ind. Pharm. 41, 875–887. https://doi.org/10.3109/03639045.2014.971027.

Jørgensen, A.C., Strachan, C.J., Pölänen, K.H., Koradia, V., Tian, F., Rantanen, J., 2009. An insight into water of crystallization during processing using vibrational spectroscopy. J. Pharm. Sci. 98, 3903–3932. https://doi.org/10.1002/jps.21735.

Kaplan, S.A., 1972. Biopharmaceutical considerations in drug formulation design and evaluation. Drug Metab. Rev. 1, 15–34. https://doi.org/10.3109/03602537208993907.

Mithu, M.S.H., Economidou, S., Trivedi, V., Bhatt, S., Douroumis, D., 2021. Advanced methodologies for pharmaceutical salt synthesis. Cryst. Growth Des. 21, 1358–1374. https://doi.org/10.1021/acs.cgd.0c01427.

Mondal, P.K., Rao, V., Mittapalli, S., Chopra, D., 2017. Exploring solid state diversity and solution characteristics in a fluorine-containing drug riluzole. Cryst. Growth. Des. 595, 1938–1946. https://doi.org/10.1021/acs.cgd.6b01894.

Moroni, A.B., Perez Mayoral, E., Lionello, D.F., Vega, D.R., Kaufman, T.S., Calvo, N.L., 2023. Characterization of the hydrochloride salt hemihydrate as a new salt of the antifungal agent tioconazole. Int. J. Pharm. 637, 122869. https://doi.org/10.1016/j.ijpharm.2023.122869.

Moroni, A.B., Perez Mayoral, E., Lionello, D.F., Vega, D.R., Kaufman, T.S., Calvo, N.L., 2023. Solid-state properties of Nifurtimox. Preparation, analytical characterization, and stability of an amorphous phase. Eur. J. Pharm. Biopharm. 184, 25–35. https://doi.org/10.1016/j.ejpb.2023.01.008.

Nowak, M., Gajda, M., Baranowski, P., Szymczyk, P., Karolewicz, B., Nartowski, K.P., 2020. Stabilisation and growth of metastable form II of fluconazole in amorphous solid dispersions. Pharmaceutics 12, 12. https://doi.org/10.3390/pharmaceutics12010012.

Petit, S., Coquerel, G., 1996. Mechanism of several solid-solid transformations between dihydrated and anhydrous copper(II) 8-hydroxyquinolinates. Proposition for a unified model for the dehydration of molecular crystals. Chem. Mater. 8, 2247–2258. https://doi.org/10.1021/cm9600438.

Rout, S.R., Kenguva, G., Giri, L., Dandela, R., 2023. Novel salts of the antiemetic drug-Domperidone: synthesis, characterization and physicochemical property investigation. CrystEngComm 25, 513–524. https://doi.org/10.1039/D2CE00902A.

Sanli, S., Basaran, F., Sanli, N., Akmese, B., Bulduk, I., 2013. Determination of dissociation constants of some antifungal drugs by two different methods at 298 K. J. Sol. Chem. 42, 1976–1987. https://doi.org/10.1007/s10953-013-0083-x.

Serajuddin, A.T.M., 2007. Salt formation to improve drug solubility. Adv. Drug Deliv. Rev. 59, 603–616. https://doi.org/10.1016/j.addr.2007.05.010.

Stratton, C.F., Newman, D.J., Tan, D.S., 2015. Cheminformatic comparison of approved drugs from natural products versus synthetic origins. Bioorg. Med. Chem. Lett. 25, 4802–4807. https://doi.org/10.1016/j.bmcl.2015.07.014.

Weng, J., Wong, S.N., Xu, X., Xuan, B., Wang, C., Chen, R., Sun, C.C., Lakerveld, R., Kwok, P.C.L., Chow, S.F., 2019. Cocrystal engineering of itraconazole with suberic acid via rotary evaporation and spray drying. Cryst. Growth Des. 19, 2736–2745. https://doi.org/10.1021/acs.cgd.8b01873.

Williams, H.D., Trevaskis, N.L., Charman, S.A., Shanker, R.M., Charman, W.N., Pouton, C.W., Porter, C.J.H., 2013. Strategies to address low drug solubility in discovery and development. Pharmacol. Rev. 65, 315–499. https://doi.org/10.1124/pr.112.005660.

Worzakowska, M., Sztanke, M., Rzymowska, J., Sztanke, K., 2023. Thermal decomposition path—studied by the simultaneous thermogravimetry coupled with Fourier transform infrared spectroscopy and quadrupole mass spectrometry of imidazoline/dimethyl succinate hybrids and their biological characterization. Materials 16, 4638. https://doi.org/10.3390/ma16134638.

Yu, L.X., Carlin, A.S., Amidon, G.L., Hussain, A.S., 2004. Feasibility studies of utilizing disk intrinsic dissolution rate to classify drugs. Int. J. Pharm. 270, 221–227. https://doi.org/10.1016/j.ijpharm.2003.10.016.